

Supplement of Atmos. Chem. Phys., 19, 12295–12307, 2019
<https://doi.org/10.5194/acp-19-12295-2019-supplement>
© Author(s) 2019. This work is distributed under
the Creative Commons Attribution 4.0 License.



Supplement of

Relative humidity and O₃ concentration as two prerequisites for sulfate formation

Yanhua Fang et al.

Correspondence to: Tong Zhu (tzhu@pku.edu.cn)

The copyright of individual parts of the supplement might differ from the CC BY 4.0 License.

Supplementary information

S1. Methodology for estimation of the mass concentrations of PM_{2.5} components

S1.1 Organic matter

5 The mass concentration of organic matter (OM) was calculated from organic carbon (OC) measurements by multiplying OC by a factor that represents the mass contributions of other elements, such as oxygen, hydrogen, and nitrogen. The OM/OC ratio varies from 1.4 to 2.2 and is expected to increase as aerosols age (El-Zanan et al., 2005). We chose a factor of 1.6 to calculate OM in Beijing following advice in the literature (Xing et al., 2013).

S1.2 Minerals

10 The total mass concentration of minerals, referred to as “minerals”, can be estimated by the following equation (Chan et al., 1997):

$$[\text{minerals}] = 2.2[\text{Al}] + 2.49[\text{Si}] + 1.63[\text{Ca}] + 2.42[\text{Fe}] + 1.94[\text{Ti}] , \quad (\text{Eq. 1})$$

where $[x]$ represents the mass concentration of species x . According to Zhang et al. (2003), on average Al accounted 7 % of total mineral dust mass concentrations in North, Northwest, and West China. Mineral concentrations can thus also be estimated by Eq. 2:

15 $[\text{minerals}] = [\text{Al}]/0.07 , \quad (\text{Eq. 2})$

We calculated $[\text{minerals}]$ with the two methods above and found no significant differences (Fig. S1). Equation 2 was therefore employed to calculate $[\text{minerals}]$ in this study.

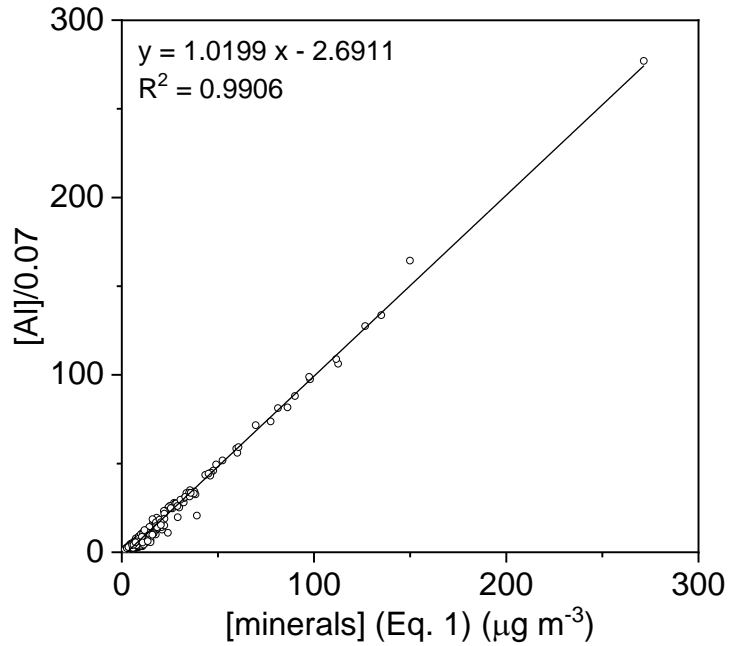


Figure S1. Comparison of the two methods for the calculation of [minerals].

S1.3 Trace element oxides

The enrichment factors (EFs) of trace element oxides (TEOs) can be used to determine whether natural or anthropogenic sources dominated our observations. The EF value of element i was defined as follows:

$$EF_i = \frac{[X_i/X_{ref}]_{\text{sample}}}{[X_i/X_{ref}]_{\text{crust}}}, \quad (\text{Eq. 3})$$

where $[X_i/X_{ref}]_{\text{sample}}$ is the mass concentration ratio of element i to the reference element in our samples and $[X_i/X_{ref}]_{\text{crust}}$ is the mass concentration ratio of element i to the reference element in average crust (Hans Wedepohl, 1995). Al was used as the reference element in this study. The EFs of each element are depicted in Fig. S2.

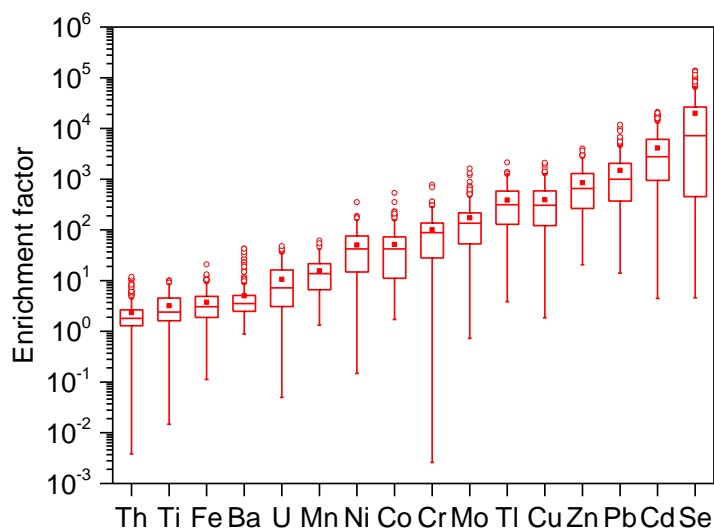


Figure S2. Elemental enrichment factors (EFs) of our samples. The boxes represent, from top to bottom, the 75th, 50th, and 25th percentiles for each element. The whiskers, solid red squares, and open red circles represent 1.5 times the interquartile range (IQR), mean values, and outlier data points, respectively.

5 If the EF was < 5, the element was considered to originate mainly from natural sources; if $5 < EF < 20$, the element originated from both natural and anthropogenic sources; if $EF > 20$, the element originated mainly from anthropogenic sources. According to Zhang et al. (2013), the mass concentrations of TEOs can be estimated by multiplied a correction factor to represent the contribution of oxygen. For elements originating from anthropogenic sources only, a factor of 1 was applied, whereas for elements of both natural and anthropogenic origin, a factor of 0.5 was applied to represent the anthropogenic part. As multiple

10 forms of metal oxides were identified, which were hard to quantify, a multiplicative factor of 1.3 was used when considering the metal abundance. The mass concentration of TEOs was calculated as described in Zhang et al. (2013):

$$[\text{TEOs}] = 1.3 \times [0.5 \times (\text{Ba} + \text{Mn} + \text{U}) + (\text{Ni} + \text{Co} + \text{Cr} + \text{Mo} + \text{Tl} + \text{Cu} + \text{Zn} + \text{Pb} + \text{Cd} + \text{Se})] , \quad (\text{Eq. 4})$$

S1.4 Aerosol water content

Aerosol water content (AWC) was calculated using the ISORROPIA-II thermodynamic model (<http://isorro피아.eas.gatech.edu>).

The Na⁺-K⁺-Ca²⁺-Mg²⁺-NH₄⁺-SO₄²⁻-NO₃⁻-Cl⁻-H₂O aerosol system was applied in reverse mode (Fountoukis and Nenes, 2007; Nenes et al., 1998).

S2 Results and discussion

S2.1 Sulfate formation mechanism

- 5 Sulfate can be formed through the oxidation of SO₂ by OH radicals in the gas phase (Stockwell and Calvert, 1983), through the oxidation of dissolved SO₂ by various oxidants (e.g., O₃, H₂O₂, NO₂, and O₂) in the aqueous phase (Seinfeld and Pandis, 2006), which may be transition metal ions (TMIs)-catalysed, or through heterogeneous reaction on the surface of sea-salt or dust aerosols (Gurciullo et al., 1999; Usher, 2002).

The rate of the SO₂ + OH reaction can be expressed as:

$$10 \quad R_{\text{SO}_2+\text{OH}} = k_0[\text{SO}_2(\text{g})][\text{OH}(\text{g})] \quad , \quad (\text{Eq. 5})$$

where k_0 is the rate constant and $[x]$ represents the concentration of species x . The production rate of sulfate through OH radical oxidation can be expressed as:

$$P_{\text{OH}} = \frac{3600 \times 96 \times p \times R_{\text{SO}_2+\text{OH}}}{RT} \quad , \quad (\text{Eq. 6})$$

- 15 where 3600 is a time conversion factor (s h⁻¹), 96 is the molar mass of SO₄²⁻ (g mol⁻¹), p is atmospheric pressure (kPa), R is the gas constant (8.31 Pa m³ mol⁻¹ K⁻¹), and T is the temperature (K).

SO₂ reacts with H₂O₂, O₃, NO₂, and O₂ (TMIs-catalysed) in the aqueous phase. The rates of the four main aqueous reactions are expressed as (He et al., 2018; Seinfeld and Pandis, 2006):

$$R_{\text{SO}_2+\text{O}_3} = (k_1[\text{SO}_2 \cdot \text{H}_2\text{O}] + k_2[\text{HSO}_3^-] + k_3[\text{SO}_3^{2-}])(\text{O}_3(\text{aq})) \quad , \quad (\text{Eq. 7})$$

$$R_{\text{SO}_2+\text{H}_2\text{O}_2} = \frac{k_4[\text{H}^+][\text{HSO}_3^-][\text{H}_2\text{O}_2(\text{aq})]}{1 + K[\text{H}^+]} \quad , \quad (\text{Eq. 8})$$

$$20 \quad R_{\text{SO}_2+\text{NO}_2} = k_5[\text{S(IV)}][\text{NO}_2(\text{aq})] \quad , \quad (\text{Eq. 9})$$

$$R_{\text{SO}_2+\text{O}_2} = k_6[\text{H}^+]^{-0.74} [\text{S(IV)}][\text{Mn(II)}][\text{Fe(III)}] \quad (\text{pH} < 4.2) \quad , \quad (\text{Eq. 10})$$

$$R_{\text{SO}_2+\text{O}_2} = k_7 [\text{H}^+]^{0.67} [\text{S(IV)}][\text{Mn(II)}][\text{Fe(III)}] \quad (\text{pH} > 4.2) , \quad (\text{Eq. 11})$$

The production rate of sulfate through aqueous oxidation routes can be expressed as:

$$P_{\text{aqu}(\text{ox}_i)} = 3600 \times 96 \times R_{\text{SO}_2+\text{ox}_i} \times \frac{\text{LWC}}{\rho_{\text{H}_2\text{O}}} , \quad (\text{Eq. 12})$$

where k_n ($n = 1-7$) is the rate constant of each oxidation route, $K = 13 \text{ M}^{-1}$ at 298 K, LWC is the liquid water content (mg m^{-3}), $\rho_{\text{H}_2\text{O}}$ is the density of water (1 kg L^{-1}), and ox_i ($i = \text{O}_3, \text{H}_2\text{O}_2, \text{NO}_2, \text{and O}_2$) represents different oxidants.

The heterogeneous reaction rate $R_{\text{het}(\text{ox}_i)}$ can be expressed as (Jacob, 2000; Wang et al., 2012; Zheng et al., 2015):

$$R_{\text{het}(\text{ox}_i)} = k_{\text{ox}_i} [\text{SO}_2(\text{g})] , \quad (\text{Eq. 13})$$

where

$$k_{\text{ox}_i} = \left(\frac{d_p}{2D_i} + \frac{4}{v_i \gamma_i} \right)^{-1} S_p , \quad (\text{Eq. 14})$$

d_p is the effective diameter of the particles (m), D_i is the gas phase molecular diffusion coefficient ($\text{m}^2 \text{ s}^{-1}$), v_i is the mean molecular speed in the gas phase (m s^{-1}), and S_p is the aerosol surface area ($\text{m}^2 \text{ m}^{-3}$). The uptake coefficient γ_i depends on RH:

$$\gamma_i = \left\{ \begin{array}{ll} \gamma_{\text{low}} & 0 < \text{RH} \leq 50 \% \\ \gamma_{\text{low}} + \frac{(\gamma_{\text{high}} - \gamma_{\text{low}})(\text{RH} - 0.5)}{\text{RH}_{\text{max}} - 0.5} & 50 \% < \text{RH} \leq \text{RH}_{\text{max}} \\ \gamma_{\text{high}} & \text{RH}_{\text{max}} < \text{RH} \leq 100 \% \end{array} \right\} \quad (\text{Eq. 15})$$

where γ_{low} and γ_{high} can be obtained from Wang et al. (2012) and RH_{max} is the RH at which γ reaches γ_{high} . The rate of sulfate production via heterogeneous reactions $P_{\text{het}(\text{ox}_i)}$ can be expressed as:

$$P_{\text{het}(\text{ox}_i)} = \frac{3600 \times 96 \times p \times R_{\text{het}(\text{ox}_i)}}{RT} , \quad (\text{Eq. 16})$$

S2.2 Influencing parameters

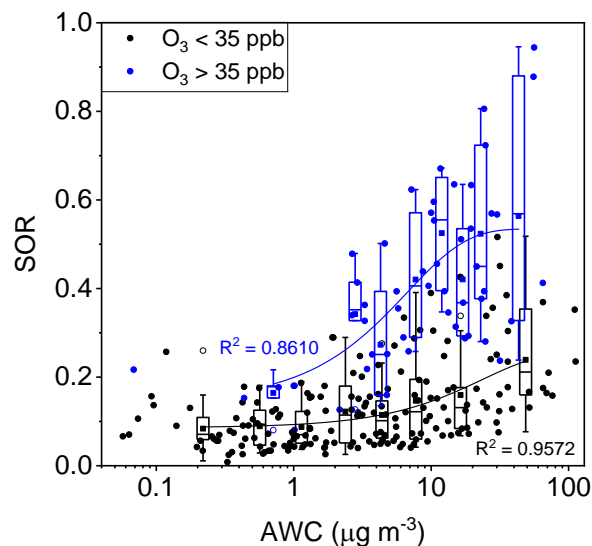


Figure S3. Plot of the SOR against aerosol water content (AWC) (note log scale), grouped by O₃ concentration. The solid blue circles represent O₃ > 35 ppb and the solid black circles represent O₃ < 35 ppb. The boxes represent, from top to bottom, the 75th, 50th, and 25th percentiles in each bin, which were also separated according to the 35 ppb O₃ concentration threshold; the bin widths were set such that there were an approximately equal number of data points in each bin. The whiskers, solid squares, and open circles represent 1.5 times the IQR, mean values, and outlier data points, respectively. The lines are best fits to the mean values based on a sigmoid function. Data for days with rain or snow were excluded from this plot.

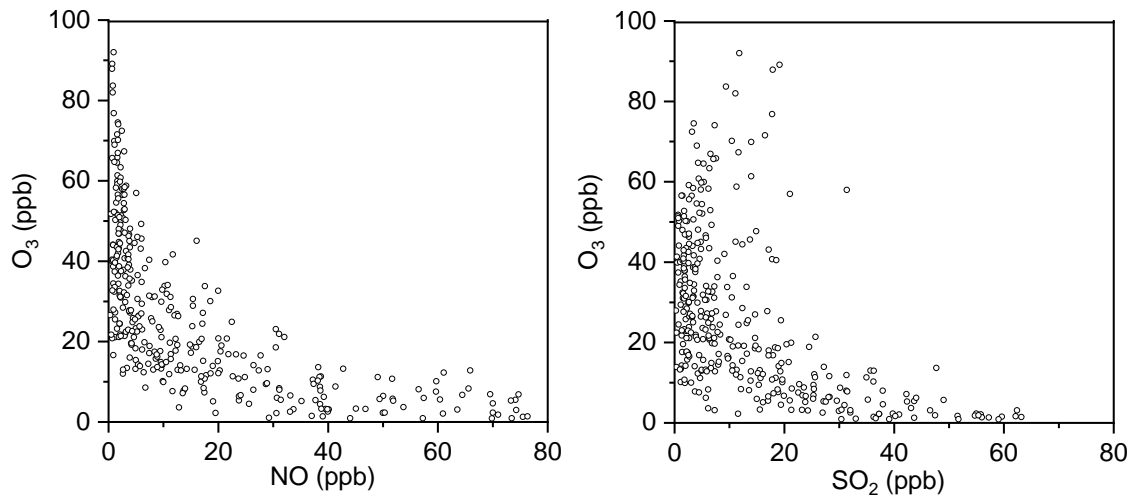


Figure S4. Plots of O_3 against the primary emission tracers NO and SO_2 .

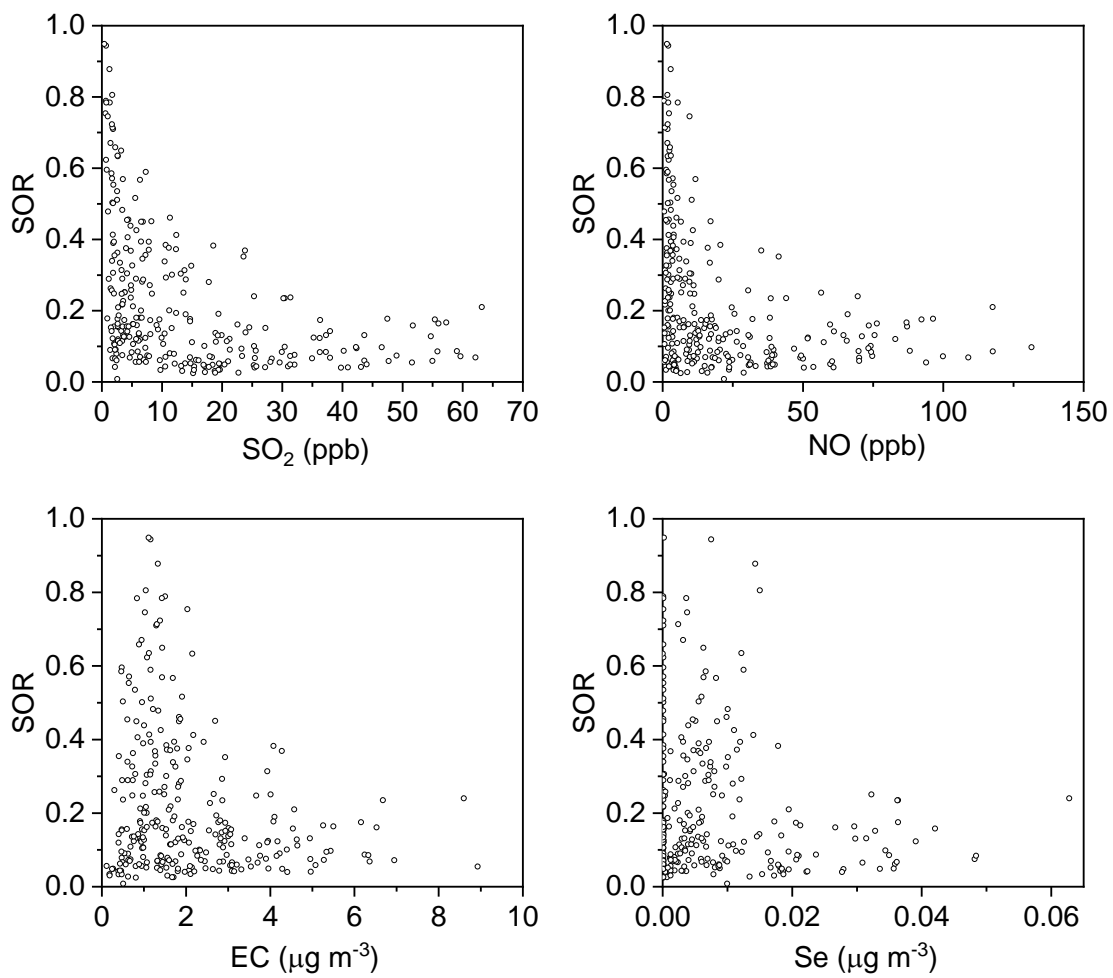


Figure S5. Plots of sulfur oxidation ratios (SORs) against the primary emission tracers SO_2 , NO, EC, and Se.

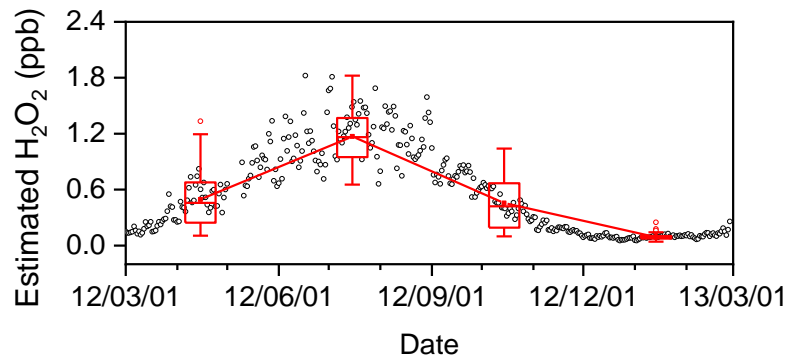


Figure S6. Time series of estimated H_2O_2 from March 1 2012 to February 28 2013. H_2O_2 was estimated from temperature (T) based on the fitting function $\text{H}_2\text{O}_2 = 0.1155e^{0.0846T}$ according to Fu (2014). The boxes represent, from top to bottom, the 75th, 50th, and 25th percentiles for each season. The whiskers, solid red squares, and open red circles represent 1.5 times the interquartile range (IQR), seasonal mean values, and outlier data points, respectively.

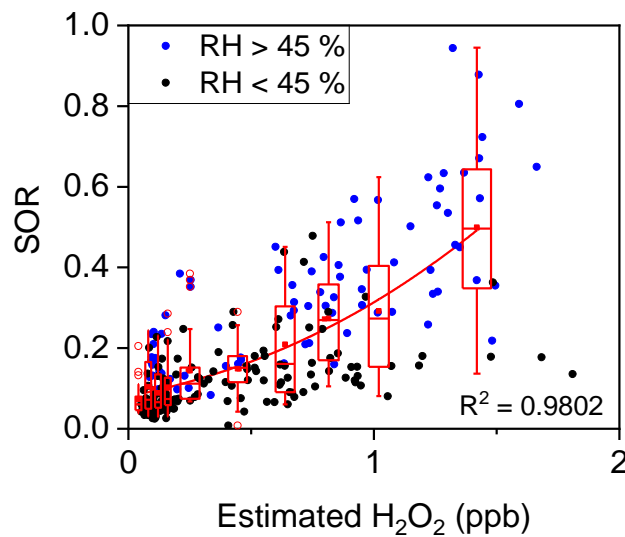


Figure S7. Plot of the SOR against estimated H_2O_2 grouped by RH. The solid blue circles represent $\text{RH} > 45\%$ and the solid black circles represent $\text{RH} < 45\%$. The boxes represent, from top to bottom, the 75th, 50th, and 25th percentiles in each bin. The bin widths were set such that there were an approximately equal number of data points in each bin. The whiskers, solid squares, and open circles represent 1.5 times

the IQR, mean values, and outlier data points, respectively. The line are best fits to the mean values based on an exponential function. Data for days with rain were excluded from this plot.

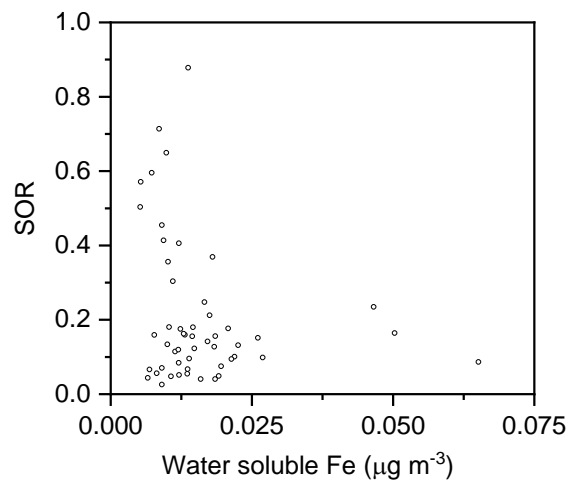


Figure S8. Plot of the SOR against water soluble Fe (54 samples selected every 6 days throughout the sampling period).

S2.3 Seasonal variations

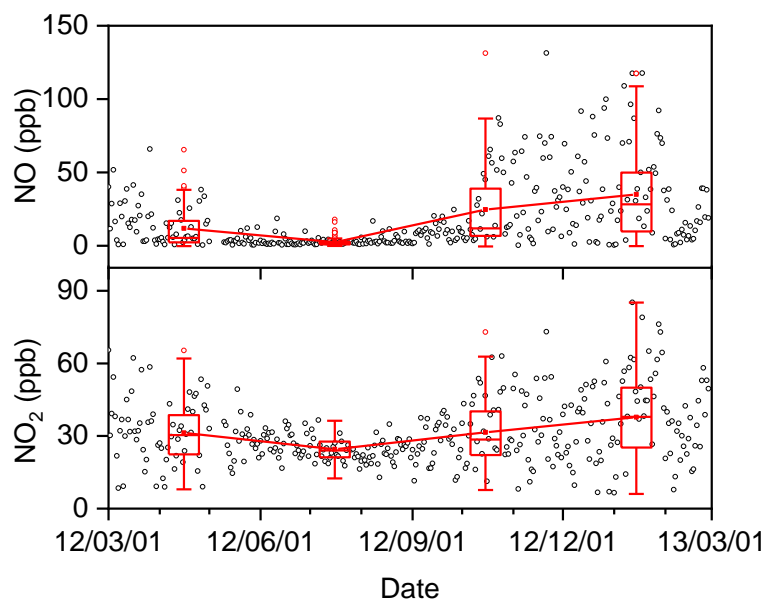


Figure S9. Time series of NO and NO₂ from March 1 2012 to February 28 2013 (open black circles). The boxes represent, from top to bottom, the 75th, 50th, and 25th percentiles for each season. The whiskers, solid red squares, and open red circles represent 1.5 times the IQR, seasonal mean values, and outlier data points, respectively.

5

References

- Chan, Y. C., Simpson, R. W., McTainsh, G. H., Vowles, P. D., Cohen, D. D., and Bailey, G. M.: Characterisation of chemical species in PM_{2.5} and PM₁₀ aerosols in Brisbane, Australia, *Atmos. Environ.*, 31, 3773-3785, [https://doi.org/10.1016/S1352-2310\(02\)00804-X](https://doi.org/10.1016/S1352-2310(02)00804-X), 1997.
- 5 El-Zanan, H. S., Lowenthal, D. H., Zielinska, B., Chow, J. C., and Kumar, N.: Determination of the organic aerosol mass to organic carbon ratio in IMPROVE samples, *Chemosphere*, 60, 485-496, <https://doi.org/10.1016/j.chemosphere.2005.01.005>, 2005.
- Fountoukis, C., and Nenes, A.: ISORROPIA II: a computationally efficient thermodynamic equilibrium model for K⁺-Ca²⁺-Mg²⁺-NH₄⁺-Na⁺-SO₄²⁻-NO₃⁻-Cl⁻-H₂O aerosols, *Atmos. Chem. Phys.*, 7, 4639-4659, [https://doi.org/10.5194/acp-7-4639-](https://doi.org/10.5194/acp-7-4639-2007)
10 2007, 2007.
- Fu, A.: Study on peroxide concentration and its influence factors in the urban atmosphere, Master, College of Environmental and Resource Sciences, Zhejiang University, Hangzhou, China, 2014 (in Chinese).
- Gurciullo, C., Lerner, B., Sievering, H., and Pandis, S. N.: Heterogeneous sulfate production in the remote marine environment: Cloud processing and sea-salt particle contributions, *J. Geophys. Res.*, 104, 21719, <https://doi.org/10.1029/1999jd900082>,
15 1999.
- Hans Wedepohl, K.: The composition of the continental crust, *Geochim. Cosmochim. Ac.*, 59, 1217-1232, [https://doi.org/10.1016/0016-7037\(95\)00038-2](https://doi.org/10.1016/0016-7037(95)00038-2), 1995.
- He, P., Alexander, B., Geng, L., Chi, X., Fan, S., Zhan, H., Kang, H., Zheng, G., Cheng, Y., Su, H., Liu, C., and Xie, Z.: Isotopic constraints on heterogeneous sulfate production in Beijing haze, *Atmos. Chem. Phys.*, 18, 5515-5528, <https://doi.org/10.5194/acp-18-5515-2018>,
20 2018.
- Jacob, D. J.: Heterogeneous chemistry and tropospheric ozone, *Atmos. Environ.*, 34, 2131-2159, [https://doi.org/10.1016/s1352-2310\(99\)00462-8](https://doi.org/10.1016/s1352-2310(99)00462-8), 2000.
- Nenes, A., Pandis, S. N., and Pilinis, C.: ISORROPIA: A new thermodynamic equilibrium model for multiphase multicomponent inorganic aerosols, *Aquat. Geochem.*, 4, 123-152, <https://doi.org/10.1023/a:1009604003981>, 1998.

- Seinfeld, J. H., and Pandis, S. N.: Atmospheric chemistry and physics: From air pollution to climate change, second ed., John Wiley & Sons, New Jersey, 2006.
- Stockwell, W. R., and Calvert, J. G.: The mechanism of the HO-SO₂ reaction, *Atmos. Environ.*, 17, 2231-2235, [https://doi.org/10.1016/0004-6981\(83\)90220-2](https://doi.org/10.1016/0004-6981(83)90220-2), 1983.
- 5 Usher, C. R.: A laboratory study of the heterogeneous uptake and oxidation of sulfur dioxide on mineral dust particles, *J. Geophys. Res.*, 107, <https://doi.org/10.1029/2002JD002051>, 2002.
- Wang, K., Zhang, Y., Nenes, A., and Fountoukis, C.: Implementation of dust emission and chemistry into the Community Multiscale Air Quality modeling system and initial application to an Asian dust storm episode, *Atmos. Chem. Phys.*, 12, 10209-10237, <https://doi.org/10.5194/acp-12-10209-2012>, 2012.
- 10 Xing, L., Fu, T. M., Cao, J. J., Lee, S. C., Wang, G. H., Ho, K. F., Cheng, M. C., You, C. F., and Wang, T. J.: Seasonal and spatial variability of the OM/OC mass ratios and high regional correlation between oxalic acid and zinc in Chinese urban organic aerosols, *Atmos. Chem. Phys.*, 13, 4307-4318, <https://doi.org/10.5194/acp-13-4307-2013>, 2013.
- Zhang, R., Jing, J., Tao, J., Hsu, S. C., Wang, G., Cao, J., Lee, C. S. L., Zhu, L., Chen, Z., Zhao, Y., and Shen, Z.: Chemical characterization and source apportionment of PM_{2.5} in Beijing: Seasonal perspective, *Atmos. Chem. Phys.*, 13, 7053-7074, <https://doi.org/10.5194/acp-13-7053-2013>, 2013.
- 15 Zhang, X. Y., Gong, S. L., Shen, Z. X., Mei, F. M., Xi, X. X., Liu, L. C., Zhou, Z. J., Wang, D., Wang, Y. Q., and Cheng, Y.: Characterization of soil dust aerosol in China and its transport and distribution during 2001 ACE-Asia: 1. Network observations, *J. Geophys. Res.*, 108, <https://doi.org/10.1029/2002jd002632>, 2003.
- Zheng, B., Zhang, Q., Zhang, Y., He, K. B., Wang, K., Zheng, G. J., Duan, F. K., Ma, Y. L., and Kimoto, T.: Heterogeneous chemistry: a mechanism missing in current models to explain secondary inorganic aerosol formation during the January 2013 haze episode in North China, *Atmos. Chem. Phys.*, 15, 2031-2049, <https://doi.org/10.5194/acp-15-2031-2015>, 2015.
- 20